Fabrication of mirror arrays with an ultra-precision cutting technique for a near-infrared integral field unit SWIMS-IFU

Kushibiki, Kosuke, Hosobata, Takuya, Takeda, Masahiro, Yamagata, Yutaka, Morita, Shin-ya, et al.

Kosuke Kushibiki, Takuya Hosobata, Masahiro Takeda, Yutaka Yamagata, Shin-ya Morita, Kentaro Motohara, Shinobu Ozaki, Toshihiro Tsuzuki, Hidenori Takahashi, Yukihiro Kono, Masahiro Konishi, Natsuko M. Kato, Yasunori Terao, Hiroki Nakamura, "Fabrication of mirror arrays with an ultra-precision cutting technique for a near-infrared integral field unit SWIMS-IFU," Proc. SPIE 11451, Advances in Optical and Mechanical Technologies for Telescopes and Instrumentation IV, 114512Y (13 December 2020); doi: 10.1117/12.2560431

SPIE.

Event: SPIE Astronomical Telescopes + Instrumentation, 2020, Online Only

Fabrication of mirror arrays with an ultra-precision cutting technique for a near-infrared integral field unit SWIMS-IFU

Kosuke Kushibiki[ab], Takuya Hosobata[c], Masahiro Takeda[c], Yutaka Yamagata[c], Shin-ya Morita[d], Kentaro Motohara[ab], Shinobu Ozaki[e], Toshihiro Tsuzuki[b], Hidenori Takahashi[f], Yukihiro Kono[a], Masahiro Konishi[g], Natsuko M. Kato[g], Yasunori Terao[a], and Hiroki Nakamura[ab]

[a]Department of Astronomy, Graduate School of Science, The University of Tokyo, 7-3-1 Hongo, Bunkyo-ku, Tokyo 113-0033, Japan
[b]Advanced Technology Center, National Astronomical Observatory of Japan, 2-21-1 Osawa, Mitaka, Tokyo 181-8588, Japan
[c]RIKEN Center for Advanced Photonics (RAP), RIKEN, 2-1 Hirosawa, Wako, Saitama 351-0198, Japan
[d]Faculty of Engineering, Tokyo Denki University, 5 Senju Asahi-cho, Adachi-ku, Tokyo 120-8551, Japan
[e]Subaru telescope, National Astronomical Observatory of Japan, 2-21-1 Osawa, Mitaka, Tokyo 181-8588, Japan
[f]Kiso observatory, Institute of Astronomy, The University of Tokyo, 10762-30, Mitake, Kiso-machi, Kiso-gun,Nagano 397-0101, Japan
[g]Institute of Astronomy, Graduate School of Science, The University of Tokyo, 2-21-1 Osawa, Mitaka, Tokyo 181-0015, Japan

ABSTRACT

We are developing an image-slicer type integral field unit (IFU), SWIMS-IFU, for SWIMS (Simultaneous-color Wide-field Infrared Multi-object Spectrograph), a near-infrared instrument for TAO 6.5 m telescope. SWIMS-IFU divides a field-of-view of $16\farcs6 \times 12\farcs8$ into 26 slices with a width of $\sim 0\farcs5$, which is the largest FoV among near-infrared IFUs on 8 m class telescopes. It is also capable of obtaining entire near-infrared spectra from 0.9 to 2.5 μm with R$\sim$1000 with a single exposure. Because of limitations of space in SWIMS, SWIMS-IFU should fit in a volume of $170 \times 220 \times 60$ mm^3, which results in small and complicatedly aligned mirror facets. To reduce alignment procedures, we adopt an ultra-precision cutting technique to fabricate mirror arrays monolithically. We have completed one of the mirror arrays, the slit-mirror array which consists of 26 spherical mirror facets, and confirmed both their surface roughness and shape errors satisfy the requirements. We also have fabricated a prototype of the pupil-mirror array including some elliptical mirror facets and confirmed that the elliptical mirrors have enough surface qualities and produce better image quality than spherical ones by a pinhole imaging test.

Keywords: Integral field unit, Ultra-precision cutting, TAO 6.5-m telescope, Near-infrared spectroscopy, SWIMS

1. INTRODUCTION

Integral field spectroscopy (IFS) enables us to obtain spatially resolved spectra over an entire field of view with a single exposure and to investigate physical properties and kinematics within the field. Recently, IFS in the near-infrared wavelength is getting important to probe dust-obscured targets, such as star-forming regions and

Further author information: (Send correspondence to K.K.)
K.K.: E-mail: k.kushibiki@ioa.s.u-tokyo.ac.jp, Telephone: +81 422 34 3542

Advances in Optical and Mechanical Technologies for Telescopes and Instrumentation IV, edited by Ramón Navarro, Roland Geyl, Proc. of SPIE Vol. 11451, 114512Y
 · doi: 10.1117/12.2560431

Table 1: Specifications of SWIMS-IFU.

Observatory	TAO 6.5 m	Subaru 8.2 m
Wavelength coverage	0.9–1.45 μm (Blue) & 1.45–2.5 μm (Red)	
Spectral resolution	R$\sim$900–1400 (Blue) & R$\sim$700–1200(Red)	
Field of View	$16\farcs6 \times 12\farcs8$	$13\farcs5 \times 4\farcs8$
Pixel scale	$0\farcs126$ pix^{-1}	$0\farcs095$ pix^{-1}
Slice Width	$0\farcs5$	$0\farcs4$
Number of Slices	26	12
Throughput of IFU	$> 70\%$	
Image quality	$< 0\farcs4$	

starburst galaxies, as well as to study high-redshift objects in the rest-frame optical wavelength. Although multiple emission lines are required to investigate their detailed properties, single-exposure wavelength coverages of existing near-infrared IFS instruments are limited and in many cases multiple exposures are necessary to obtain multiple emission lines. Also, a wide field of view (FoV) is necessary to carry out efficient observations of spatially extended objects, but FoVs of existing instruments are also limited, less than $10''$ square.

Therefore, we are developing an integral field unit (IFU), SWIMS-IFU, with a full near-infrared wavelength coverage (0.9–2.5 μm) and a large FoV ($16\farcs6 \times 12\farcs8$) for a near-infrared spectrograph, SWIMS (Simultaneous-color Wide-field Infrared Multi-object Spectrograph). SWIMS is one of the first generation instruments for TAO 6.5 m telescope being constructed at the summit of Cerro Chajnantor (5640 m) by Institute of Astronomy, School of Science, the University of Tokyo.[1–4] SWIMS has a capability of multi-object spectroscopy (MOS) in the entire near-infrared wavelength range (0.9–2.5 μm) with a single exposure by dividing incident light into 0.9–1.45 μm (Blue arm) and 1.45–2.5 μm (Red arm) with a dichroic mirror.[5–7] It has a MOS Unit (MOSU) to exchange multi-object slits masks in the MOS mode, which consists of a carousel storing the masks, a robotic mask catcher arm handling them, and a focal plane dewar.[8]

SWIMS-IFU is an optical unit using an image slicer to transform SWIMS into an IFS instrument only by inserting it into a focal plane and without any modifications of SWIMS optics. SWIMS-IFU is stored in the carousel of MOSU and handled by the mask catcher arm like other slits masks. Therefore, there are a size restriction of $< 170 \times 220 \times 60$ mm^3 and a weight restriction of < 900 g. Besides, as SWIMS-IFU is operated at a cryogenic temperature (100–150 K), it must be fabricated with a single material to avoid effects caused by a difference in the coefficient of thermal expansion. Specifications of SWIMS-IFU are shown in Table 1. As SWIMS and SWIMS-IFU are also operated at Subaru telescope until the construction of TAO 6.5 m telescope is completed, the specifications for both telescopes are shown. Note that the slice width is optimized to a seeing size to achieve a wider FoV than existing IFS instruments. The number of slices when on the Subaru is smaller by a factor of two, because the number of detectors installed in SWIMS is only two per arm instead of four, and only half of the final FoV is covered. So far, we have developed optical and mechanical designs and carried out basic fabrication tests of mirror facets.[9–12]

2. DESIGN

Fig.1 shows the optical design of SWIMS-IFU. The optical system consists of pre-optics including PO0 (a flat mirror), PO1 (a doublet lens), and PO2 (a spherical mirror), and three mirror arrays. Incident light is introduced into the optics of SWIMS-IFU by PO0. PO1 and PO2 magnify a telescope focal plane by a factor of 2.75 and reimage it on a slice-mirror array (S1). The slice-mirror array, consisting of 26 flat mirror facets with different angles, divides the image into 26 rectangle channels and reflects them in different directions. The slice-mirror facets are called ch+13 to ch+1 and ch–1 to ch–13 from top to bottom. At the exit pupil of the slice-mirror array a pupil-mirror array (S2) is located. It consists of 12 spherical mirror facets at the center of the array and 14 off-axis elliptical facets at the outer sides. The off-axis elliptical mirrors reduce aberrations caused by large reflection angles in the outer-side channels. The pupil-mirror array converts F-ratio into an initial value from the telescope (F/12.2) and makes pseudo slit images on a slit-mirror array (S3). The slit-mirror array consists of 26 spherical mirror facets and reflects the light into the optics of SWIMS.[10,12]

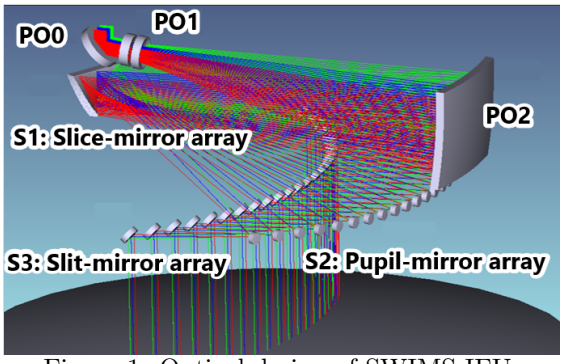

Figure 1: Optical design of SWIMS-IFU.

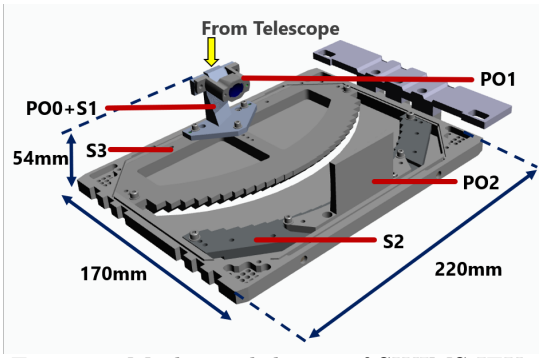

Figure 2: Mechanical design of SWIMS-IFU.

Fig.2 shows the mechanical design of SWIMS-IFU. As shown in the figure, the optical components are within a volume of $170 \times 220 \times 54$ mm^3, which satisfies the size restriction of $< 170 \times 220 \times 60$ mm^3. All the components, except for lenses of PO1, will be made of only aluminum alloys to be operated in a cryogenic condition. For the mirrors, an aluminum super alloy RSA6061 by RSP Technology, which is a finer nanostructured alloy than normal aluminum alloys, is used to achieve required surface roughness. A key point of the mechanical design is monolithic fabrication of the mirror arrays to minimize alignment procedures. PO0+S1, S2, and S3 are fabricated from a single material with an ultra-precision cutting technique, which allows us to achieve accurate relative positions of the mirror facets ($\sim \mu$m order) and surface qualities such as surface roughness and shape errors. We can also make reference surfaces for alignment of the mirror arrays with this technique.

3. FABRICATION OF SLIT AND PUPIL MIRROR ARRAYS

3.1 Fabrication Status

We fabricate the mirrors using ULG-100D(5A) of TOSHIBA Machine operated at RIKEN Center for Advanced Photonics. Final fabrication of the slit-mirror array (S3) has been completed. Test fabrication of the pupil-mirror array (S2) has been finished and its final fabrication is in progress. Fabrication of the rest of the mirrors are in preparation and will be carried out in early 2021. We will report results of the final fabrication of the slit-mirror array (S3) and the test fabrication of the pupil-mirror array (S2) in the following.

3.2 Requiements for Optical Surfaces

3.2.1 Surface roughness

A requirement for surface roughness comes from a required throughput of SWIMS-IFU since a rough surface causes scattering of light and reduces the throughput. Considering the effect of reflectivity and the scattering loss at PO0, PO2, S1, S2, and S3, the total throughput of SWIMS-IFU is written as

$$\eta = \prod_{k=1,5} R_k(\lambda) \left[1 - \left(\frac{4\pi\sigma_k}{\lambda}\right)^2\right],$$

where σ_k is the surface roughness RMS of kth surface, R_k the reflectivity, and λ an observing wavelength.[13]

To estimate the requirement for the surface roughness, we assume the reflectivity of aluminum surfaces to be $R_k(\lambda) = 0.97$, all the five facets to have the same value of surface roughness σ, and a throughput of other factors to be 90% including a vignetting at a Lyot stop of SWIMS and a throughput of the PO1 doublet lens. To achieve the total throughput of >70% at the shortest wavelength of SWIMS of 0.9 μm, the surface roughness σ must be < 10 nm, which has been confirmed as achievable in the previous fabrication tests.[11,12]

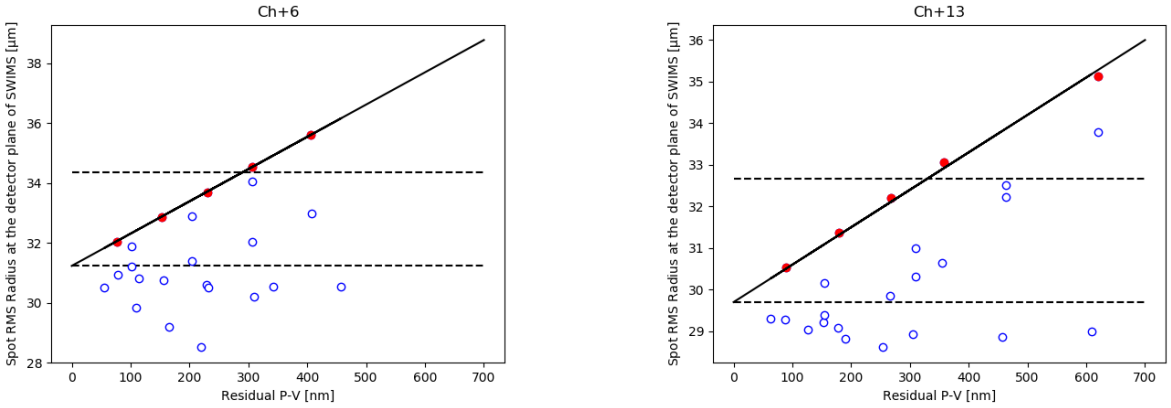

Figure 3: Relation between residual P-V values and spot RMS radii at the detector plane of SWIMS for ch+6 (left) and ch+13(right). Red filled circles show the data used in a linear fitting, and solid black line its result. The lower and upper horizontal dashed lines are design and 10% degraded spot size, respectively.

Table 2: Requirements for optical surfaces.

	Requirements
Surface roughness	RMS $<$ 10 nm
Surface shape error	P-V $<$ 300 nm

3.2.2 Surface shape error

A surface shape error is a residual peak-to-valley (P-V) value of a manufactured mirror facet from an ideal surface. A requirement for the surface shape error depends on the final image quality of SWIMS-IFU (i.e. the spot size at the SWIMS detector plane). In the following, we discuss the surface shape error of the pupil-mirror array which affects the image quality the most.

To obtain relation between the surface shape error of the pupil-mirror and the image quality, we deformed the surface shapes of ch+6 and ch+13 of the pupil-mirror array using a Zernike Standard Sag surface of ZEMAX and evaluated degradation of final spot sizes. Note that ch+6 and ch+13 have the worst final spot radius of 32 μm and 30 μm among the spherical and elliptical surfaces, respectively. We decided coefficients of the Zernike polynomial in two ways; one was that all the Zernike coefficients of defocus, two astigmatisms, two comas, two trefoils, and spherical modes were set to an equal value, and the other was that all the coefficients except for a single mode were set to zero.

Fig.3 shows the relation between the residual P-V values and spot RMS radii, where a large scatter can be seen. To evaluate the requirement conservatively, we fitted the upper edge of the plots with a linear function and set the residual P-V value at which the spot size is degraded by 10% as the requirement. As a result, the requirement for the surface shape error is P-V $<$ 300 nm.

In Table 2, the requirements for optical surfaces are summarized.

3.3 Slit-mirror Array (S3) Final Fabrication

3.3.1 Fabrication Process

The slit-mirror array (S3) consists of 26 spherical mirror facets which have different radii of curvature (61.6–65.1 mm) and tilt angles around one axis (42.2–43.5°). Each mirror facet has an aperture size of $\sim 7 \times 5$ mm^2. To fabricate the small spherical mirror facets with different curvatures, a ball end mill with a radius of 0.5 mm was used. It allows us to fabricate complicatedly aligned mirror facets in a narrow space. We used the alminum super alloy RSA6061 as a base material to achieve better surface roughness.

Fig.4 shows a configuration of the slit-mirror array fabrication when fabricating the mirror facets of the "+"-channels. When fabricating the mirror facets of the "−"-channels, the slit-mirror array is rotated 90° around the

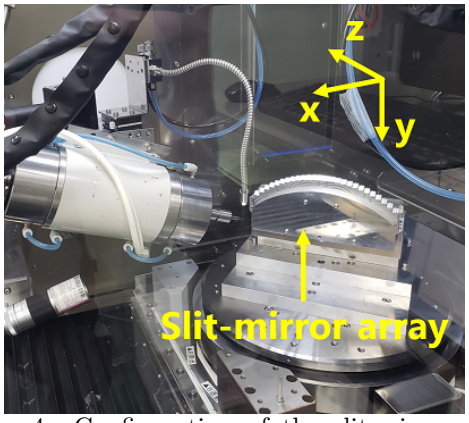

Figure 4: Configuration of the slit-mirror array fabrication when fabricating the "+"-channel mirror facets. X, Y, Z axes are those of the machine.

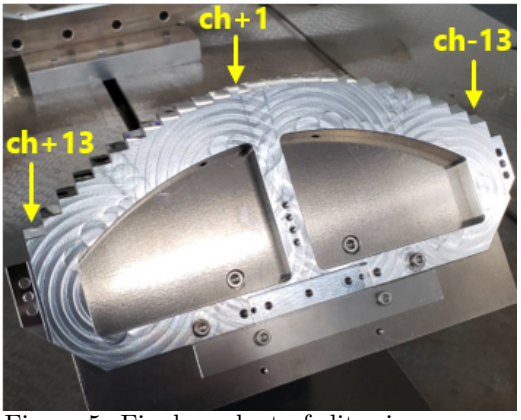

Figure 5: Final product of slit-mirror array.

Table 3: Parameters for the finishing process of the slit-mirror array.

Machine	ULG-100D(5A) (TOSHIBA Machine)
Tool	Diamond ball end mill (R∼0.5 mm)
Rotation speed	20,000 rpm
Number of the simultaneously controlled axes	3
Feed rate	100 mm/min
Pitch	10 μm
Cut in depth	2 μm

y-axis from the configuration of Fig.4. This fabrication process is necessary to avoid interference between the steps of the slit-mirror array and the ball end mill. In this configuration, simultaneous control of x, y, and z axes is necessary to cut on the tilted surface. This may be a cause of a larger control error. Fabrication parameters used in a finishing process are listed in Table 3.

3.3.2 Surface Measurements

Fig.5 shows the final product of the slit-mirror array. The surface roughness was measured by a white light interferometer, NewView 7200 (Zygo Corporation). We measured three 702 × 526 μm regions of each mirror facet that are at the center and 2 mm apart from the center to both sides along a pseudo slit direction, and obtained 78 data points in total. We fitted the data and subtracted the underlying spherical shape. Fig.6 shows surface profiles of ch+1 and ch+13 of the slit-mirror array after the subtraction. Cutter marks by the ball end mill can be seen as vertical stripes. We performed a Fourier analysis and removed low spatial frequency patterns with a spatial period of > 20 μm, which is not considered as the surface roughness, and then calculated a RMS value as the surface roughness.

The obtained surface roughness are listed in Table 4. The mean value of the 78 measurements is 7.36 nm and satisfies the requirement of < 10 nm, but 7 data points out of 78 ($\sim 9\%$) exceed the requirement. Since the requirement is for the average values of 5 mirrors in SWIMS-IFU, we have concluded that the fraction of $\sim 9\%$ doesn't have a large impact on the total throughput of SWIMS-IFU.

The surface shape was measured by a Fizeau interferometer, Verifire QPZ (Zygo corporation). We subtraceted a sphere with design values from the data. Since P-V values are strongly affected by noises in the data, we removed them with a 5σ clipping and discarded the data at the edge. We then calculated a P-V value as a surface shape error.

The results of the surface shape error are listed in Table 4. All the mirror facets satisfiy the requirement.

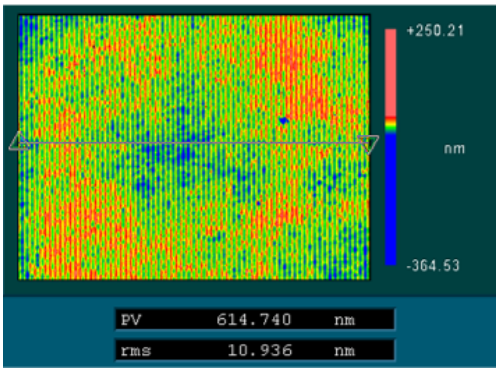

(a) ch+1

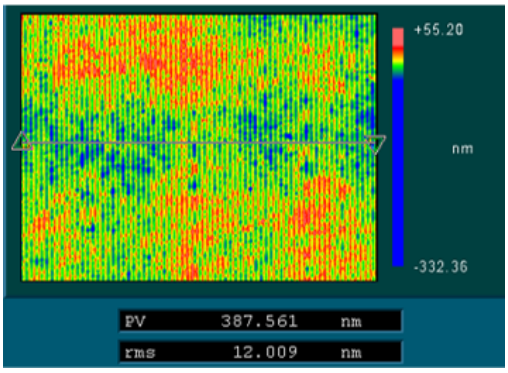

(b) ch+13

Figure 6: Residual surface profiles of 702 × 526 μm areas of (a)ch+1 and (b)ch+13 of the slit-mirror array. Spherical components are subtracted.

Table 4: Surface qualities of the slit-mirror array.

	Mean±SD	Max	Min	Requirement
Surface roughness [nm]	7.36±2.12	12.84	4.42	< 10
Surface shape error [nm]	169±32	277	117	< 300

3.4 Pupil-mirror Array (S2) Test Fabrication

3.4.1 Fabrication Process

The pupil-mirror array (S2) consists of 12 spherical mirror facets for the central channels (ch–6 to ch+6) and 14 elliptical mirror facets for the outer-side channels (ch–13 to ch–7 and ch+7 to ch+13). The spherical mirror facets have the same radius of curvature (70 mm) and the elliptical mirror facets are designed so that the two foci of the elliptical lie at the corresponding slice-mirror and slit-mirror. All the mirror facets have different tilt angles around two axes. The size of facets is $\sim 4.5 \times 7$ mm^2.

Purposes of the test fabrication are to establish a fabrication procedure of the pupil-mirror array and an experimental fabrication of the elliptical mirror facets. To evaluate quality of the elliptical mirror facets, we carried out a pinhole imaging test as the elliptical mirror facets could not be measured correctly with interferometers. Surface roughness is not an objective of this test fabrication, as we used a normal aluminum alloy, A6061, as a base material, which doesn't provide good surface roughness.

As the pupil-mirror array also has small and complicatedly aligned mirror facets like the slit-mirror array, we used a ball end mill with a radius of 1.0 mm, which was larger than that used in the slit-mirror array fabrication. The larger radius of the tool is acceptable owing to smaller effective radii of the mirror facets and is expected to provide better surface roughness in final fabrication. Fig.8 shows a configuration of the pupil-mirror array fabrication and Table 5 parameters for a finishing process of the pupil-mirror array. The biggest difference from the slit-mirror array fabrication is that the number of simultaneously controlled axes is two instead of three. The smaller number of axes results in a more stable machine control and better surface qualities.

3.4.2 Surface Measurement

We measured surface shapes of the pupil-mirrors only for spherical mirror facets (ch–6 to ch+6) with the same interferometer as that used for the slit-mirror array. To remove noises affecting P-V values, edge regions of the data were discarded. We fitted the data with the piston, tilt, and defocus modes of the Zernike polynomial and subtracted to get a residual, assuming the modes of the Zernike polynomial are systematic patterns caused by the measurement. Then we calculated a P-V value of the residual as a surface shape error. Fig.10 shows the residual surface profiles of ch+1 and ch+6.

Table 6 shows the summary of the surface shape error measurements. The average of 142 nm and the maximum of 183 nm satisfy the requirement and are smaller than those of the slit-mirror array, which may be due to the smaller number of simultaneously controlled axes.

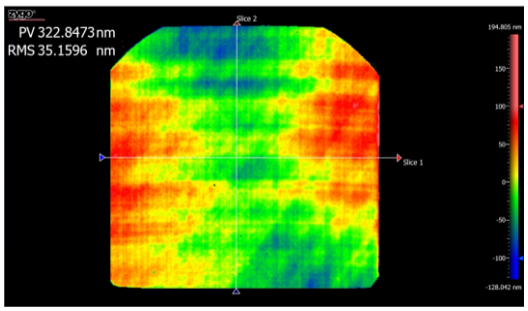

(a) ch+1

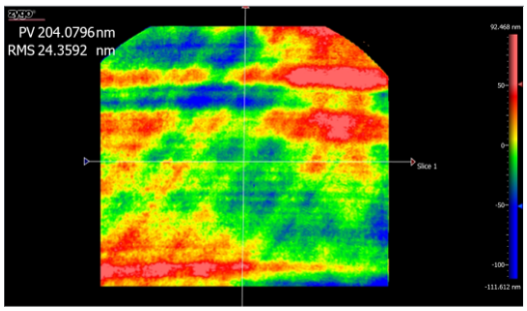

(b) ch+13

Figure 7: Residual surface profiles of (a)ch+1 and (b)ch+13 of the slit-mirror array.

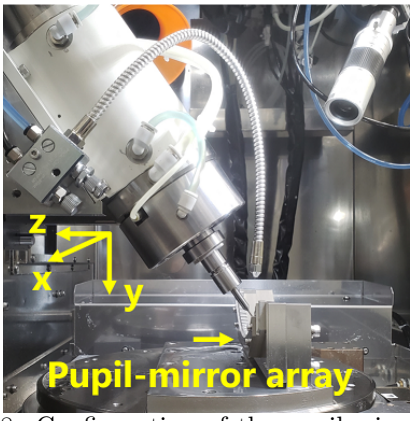

Figure 8: Configuration of the pupil-mirror array fabrication. X, Y, Z axes are the axes of the machine.

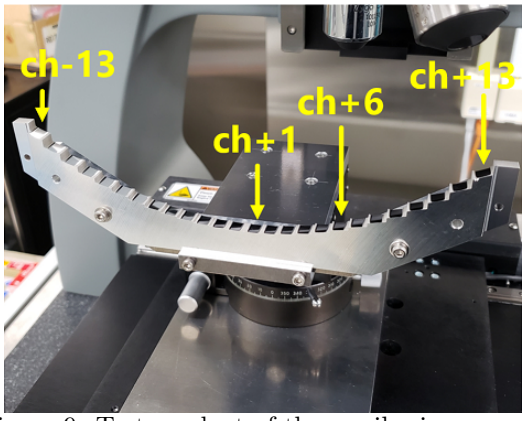

Figure 9: Test product of the pupil-mirror array.

3.4.3 Pinhole Imaging Test

We carried out a pinhole imaging test of the pupil-mirror array to evaluate imaging quality of the mirror facets and an effect of diffraction light caused by the cutter marks on their surfaces.

The setup is shown in Fig.11. The light source is a He-Ne laser (633 nm), which is converted to a beam with F/33.5 by a spatial filter and a diaphragm. The light is reflected by a pupil-mirror and an image of a pinhole in the spatial filter with a diameter of 25 μm is created on a flat mirror. The light reflected by the flat mirror is reimaged on a CMOS detector by a camera lens. The setup was designed to reproduce the situation that a point source on the slice-mirror array is reimaged on the slit-mirror array by the pupil-mirror array. Magnification factors of the pupil-mirror and the camera lens are 1/2.75 and 1/1.67 respectively, thus an ideal size of the pinhole image on the CMOS detector is 5.44 μm. Note that the pixel size of the CMOS detector is 3.45 μm/pix which is undersample considering the pinhole spot size.

We carried out the test for ch$\pm$1, $\pm$6, $\pm$7, and $\pm$13. The former two are spherical mirror facets and the latter two are elliptical. Fig.12 and 13 show the FWHMs and pinhole images, respectively. The pinhole images by the elliptical mirror facets show smaller FWHMs and better spot shapes than those by the spherical mirror facets. Therefore, we conclude that the elliptical mirror facets are fabricated correctly and improve the image quality as designed. Note that the worst FWHM of ch–6 may be caused by misalignment and some FWHMs smaller than the ideal size of 5.44 μm may be due to the undersampling effect.

For ch$\pm$13, we could place the CMOS detector at the position of the flat mirror in Fig.11 and get images of $\pm$1st order diffraction light, shown in Fig.14. Each image is created by combining 20 images with an exposure time of 50 μs. Locations of the diffraction light are perpendicular to the cutter marks. We carried out photometries of the diffraction light with apertures drawn as white circles in Fig.14 and the results are listed in Table 7.

Table 5: Parameters for the finishing process of the pupil-mirror array.

Machine	ULG-100D(5A) (TOSHIBA Machine)
Tool	Diamond ball end mill (R∼1.0 mm)
Rotation speed	24,000 rpm
Number of the simultaneous controlled axes	2
Feed rate	100 mm/min
Pitch	10 μm
Cut in depth	2 μm

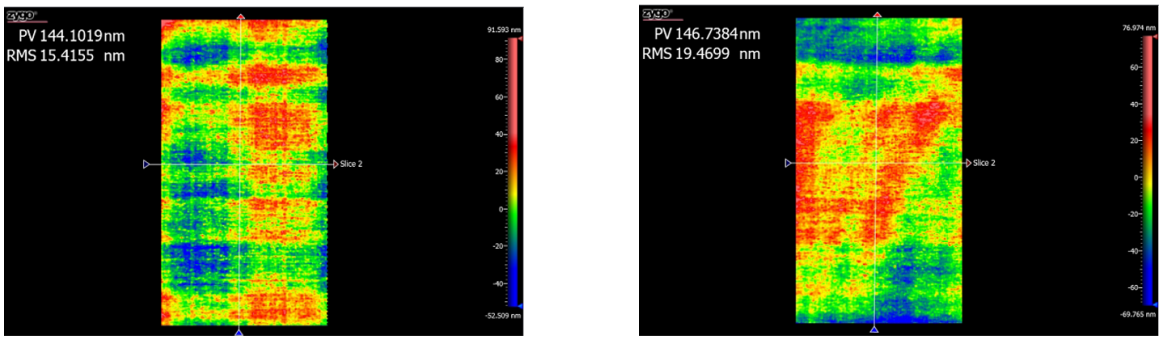

(a) ch+1 (b) ch+6

Figure 10: Residual surface profiles of (a)ch+1 and (b)ch+6 of the pupil-mirror array.

The ratios of the ±1st order diffraction light to the 0th order light are less than 1%, therefore the effect of the diffraction light is negligible.

4. SUMMARY AND FUTURE TASKS

We have been developing a near-infrared integral field unit, SWIMS-IFU, for a near-infrared spectrograph SWIMS. The optical components are developed by an ultra-precision cutting technique. The final fabrication of the slit-mirror array (S3) has been completed and the qualities such as surface roughness and surface shape errors satisfy the requirements. This is the first completion of the optical components of SWIMS-IFU. We also carried out the test fabrication of the pupil-mirror array (S2). By the simultaneous 2-axes control, we achieve a smaller surface shape error than that of the slit-mirror array. With the pinhole imaging test, we confirm that the elliptical mirror facets are fabricated correctly and the effect of the 1st order diffraction light caused by cutter marks is negligible.

The next fabrication is PO0+S1. It will be fabricated with a shaper cutting process. In the fabrication, tools for the PO0 flat mirror and the slice-mirrors will be simultaneously installed to the cutting machine, and fabrications of the two kinds of mirrors will be done in a series of processes. This fabrication will be carried out in early 2021. Assembly and performance evaluation at the lab will be done in 2021 and we plan to carry out an on-sky performance evaluation in 2022.

ACKNOWLEDGMENTS

This research is funded by a supplementary budget for economic stimulus packages formulated by Japanese government. Part of the development is supported by Ministry of Education, Culture, Sports, Science and Technology of Japan, Grant-in-Aid for Scientific Research (15H02062, 23540261, 24103003, 24244015, 2611460, 266780, 20H00171, and 20J21493) from the JSPS of Japan, and by the grant of Joint Development Research supported by the Research Coordination Committee, National Astronomical Observatory of Japan (NAOJ). KK is financially supported by Grant-in-Aid for JSPS Fellows. The development activities are supported by the Advanced Technology Center, NAOJ. The experimental setup of this work is constructed with the support from Advanced Manufacturing Support Team, RIKEN.

Table 6: Surface shape error of pupil-mirror array only for spherical surfaces.

	Mean±SD	Max	Min	Requirement
Surface shape error P-V [nm]	142±18	183	120	< 300

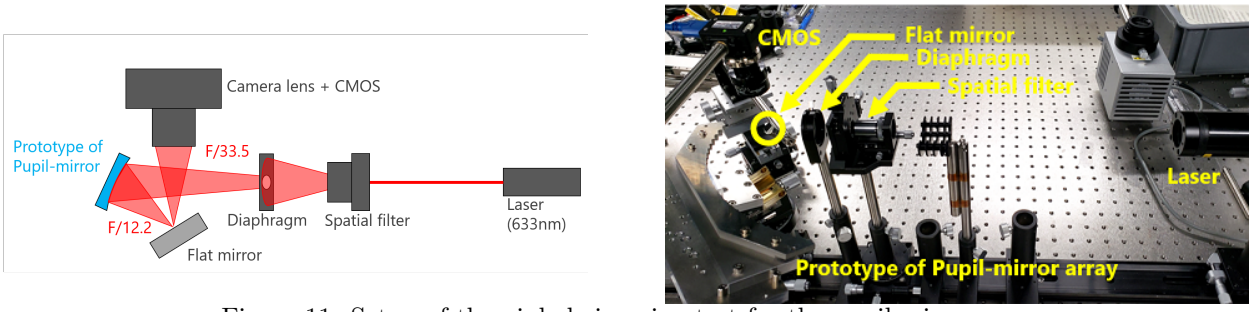

Figure 11: Setup of the pinhole imaging test for the pupil-mirror array.

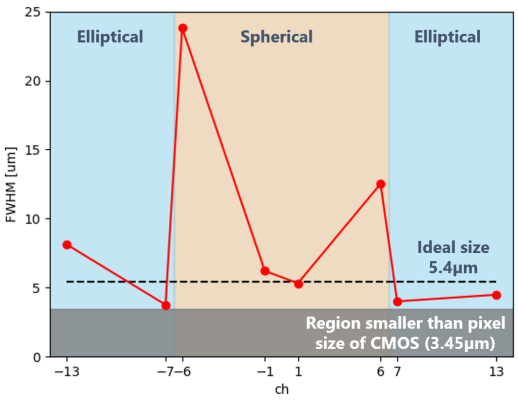

Figure 12: FHWM of the pinhole images reimaged by different channels of the pupil-mirror array.

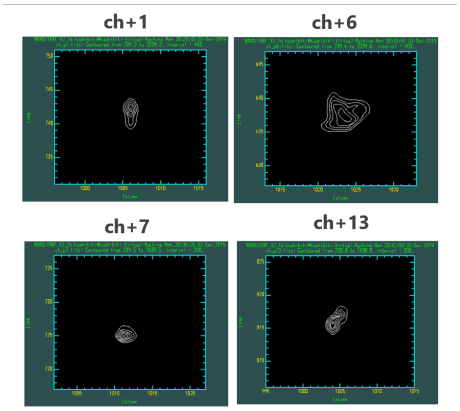

Figure 13: Contours of the pinhole images for "+"-channels.

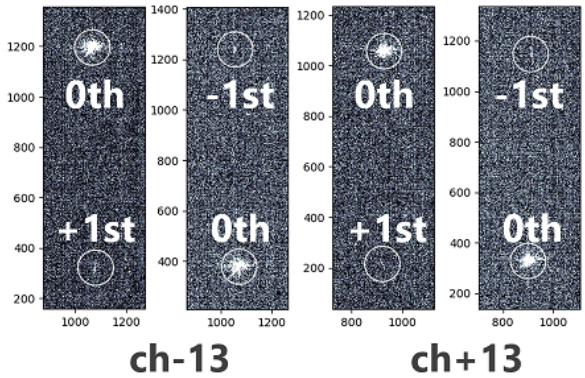

Figure 14: Images of ±1st order diffraction light with 0th order light for ch±13. White circles are apertures for photometry.

Table 7: Intensity of the diffraction light.

	0th	1st	1st/0th
ch−13 +1st	152113.1	378.7	0.00249
ch−13 −1st	129010.0	98.4	0.00076
ch+13 +1st	114899.9	34.6	0.00030
ch+13 −1st	106940.0	19.5	0.00018

REFERENCES

[1] Yoshii, Y. et al., "The University of Tokyo Atacama Observatory 6.5m telescope project," *Proc. of SPIE* **7733**, 773308 (2010).

[2] Yoshii, Y. et al., "Overview of University of Tokyo Atacama Observatory 6.5m telescope project," *Proc. of SPIE* **9145**, 914507 (2014).

[3] Yoshii, Y. et al., "The University of Tokyo Atacama Observatory 6.5m telescope: project overview and current status," *Proc. of SPIE* **9906**, 99060R (2016).

[4] Doi, M. et al., "The University of Tokyo Atacama Observatory 6.5m telescope: project overview and current status," *Proc. of SPIE* **10700**, 107000W (2018).

[5] Motohara, K. et al., "Development of a simultaneous two-color near-infrared multi-object spectrograph SWIMS for the TAO 6.5-m telescope," *Proc. of SPIE* **9147**, 91476K (2014).

[6] Motohara, K. et al., "NIR camera and spectrograph SWIMS for TAO 6.5m telescope: overview and development status," *Proc. of SPIE* **9908**, 99083U (2016).

[7] Konishi, M. et al., "Development status of the simultaneous two-color near-infrared multi-object spectrograph SWIMS for the TAO 6.5m telescope," *Proc. of SPIE* **10702**, 1070226 (2018).

[8] Takahashi, H. et al., "Development of multi-object spectroscopy unit for simultaneous-color wide-field infrared multi-object spectrograph," *Proc. of SPIE* **9147**, 91476N (2014).

[9] Ozaki, S. et al., "Development of an integral field unit for a near-infrared multi-object imaging spectrograph SWIMS," *Proc. of SPIE* **8450**, 84503Y (2012).

[10] Kitagawa, Y. et al., "Concept and optical design of the near-infrared integral field unit for SWIMS," *Proc. of SPIE* **9151**, 91514P (2014).

[11] Kitagawa, Y. et al., "Fabrication of a wide-field NIR integral field unit for SWIMS using ultra-precision cutting," *Proc. of SPIE* **9912**, 991225 (2016).

[12] Kono, Y. et al., "Design of an integral field unit for SWIMS and its milling process fabrication with an ultra-high precision machine tool," *Proc. of SPIE* **10706**, 107063F (2018).

[13] Allington-Smith, J. R. et al., "New techniques for integral field spectroscopy - I. Design, construction and testing of the GNIRS IFU," *Mon. Not. R. Astron. Soc.* **371**, 380–394 (2006).